Available online at www.sciencedirect.com
ScienceDirect
Thin Solid Films 516 (2008) 4342–4350
www.elsevier.com/locate/tsf

Spectroscopic ellipsometry and photoluminescence measurements of as-deposited and annealed silicon rich oxynitride films

Sandeep Kohli [a,*], Jeremy A. Theil [b], Patrick R. McCurdy [a], Patricia C. Dippo [c], Richard K. Ahrenkiel [c,d], Christopher D. Rithner [a], Peter K. Dorhout [a]

[a] Department of Chemistry, Colorado State University, Fort Collins, CO 80523, USA
[b] Philips Lumileds Lighting Company, LLC, 370 W. Trimble Road, MS 91MLSan Jose, CA 95131, USA
[c] Measurements and Characterization Division, National Renewable Energy Laboratory, 1617 Cole Boulevard, Golden, CO 80401, USA
[d] Department of Metallurgical and Materials Engineering, Colorado School of Mines, Golden, CO 80401, USA

Received 11 April 2007; received in revised form 12 December 2007; accepted 12 December 2007
Available online 23 December 2007

Abstract

As-deposited and annealed amorphous SiO_xN_y/H ($0.17 \le x \le 0.96$; $0.07 \le y \le 0.27$) films were characterized by spectroscopic ellipsometry and room temperature photoluminescence measurements. The refractive index of as-deposited silicon oxynitride films could be successfully varied between SiO_2 and a-Si with increased silicon content. As-deposited films were annealed under inert conditions at 400–800 °C for 4 h. Annealing conditions were insufficient to nucleate silicon nanocrystals in the films. High temperature annealing facilitated the hydrogen diffusion out of the film. This led to the reduced thickness and increased refractive index of the silicon rich oxynitride film. A correlation was seen between the changes in the refractive index, optical band gap, E_{04} (energy corresponding to an absorption coefficient of 10^4 cm^{-1}) and Urbach Energy as a function of composition and annealing conditions. The influence of annealing conditions on the photoluminescence spectra of silicon rich oxynitride films has been investigated. The room temperature luminescence in annealed $SiO_{0.96}N_{0.27}$:H films was attributed to the formation of oxygen related defects in these films. In other films, the bonded hydrogen as well as silicon and nitrogen content, played an extremely important role in determining the influence of annealing conditions on the photoluminescence spectra.

Keywords: Silicon rich oxynitride; Spectroscopic ellipsometry; Photo luminescence

1. Introduction

Amorphous silicon rich oxynitride (SRON) films are composed of silicon, oxygen and nitrogen with excess silicon. Silicon oxynitride films exhibit large variations in their refractive indices with a corresponding change in their composition [1,2]. These films also effectively retard dopant diffusion through the gate dielectric that may degrade the performance of a metal-oxide-semiconductor field effect transistor [3]. Recently, we reported a detailed investigation of the chemical, vibrational and room temperature luminescence properties of as-deposited SiO_xN_y:H ($0.17 \le x \le 0.96$; $0.07 \le y \le 0.27$) films [4]. We had also successfully nucleated Silicon nanocrystals in thermally annealed $SiO_{0.17}N_{0.07}$:H films [5].

Continuing our previous studies, we report herein variable angle and variable wavelength spectroscopic ellipsometry (SE) measurements in the UV–VIS–NIR range of the low temperature plasma enhanced chemical vapor deposited (PECVD) SiO_xN_y:H ($0.17 \le x \le 0.96$; $0.07 \le y \le 0.27$) films [4,6]. SE and room temperature photoluminescence (PL) measurements are also reported for the films annealed under inert conditions in the temperature range 400–800 °C. Glancing angle X-ray diffraction (GAXRD), Fourier

* Corresponding author. Tel.: +1 970 491 4076; fax: +1 970 491 1801.
E-mail address: sandeep.kohli@colostate.edu (S. Kohli).

0040-6090/$ - see front matter © 2007 Elsevier B.V. All rights reserved.
doi:10.1016/j.tsf.2007.12.119

Transform Infrared (FTIR) spectroscopy, Scanning Electron Microscopy (SEM) and X-ray photoelectron spectroscopy (XPS) were used to complement this study.

2. Experimental details

Amorphous SiO_xN_y:H ($0.17 \le x \le 0.96$; $0.07 \le y \le 0.27$) films were deposited on Si(100) wafers with a 500 nm SiO_2 interlayer using a low temperature PECVD process [6]. The stiochiometry and FTIR analysis of these films were reported in our earlier studies [4]. Films were annealed under inert conditions under an argon flow of 100–120 sccm. The temperature of the furnace was ramped at 100 °C/h to 200 °C and remained isothermal for 2 h. Subsequently the furnace was ramped to the desired temperature (400, 600, 800 °C) and films were annealed for 4 h. Finally, the furnace was ramped down to room temperature at a rate of 50 °C/h. The furnace was continuously purged with argon gas during the entire annealing experiment.

Variable angle spectroscopic ellipsometry data for as-deposited and annealed SRON films, were acquired using a J.A. Woollam VASE ellipsometer in the wavelength range 300–1200 nm (energy range 4.13–1.03 eV) at angle of incidences of

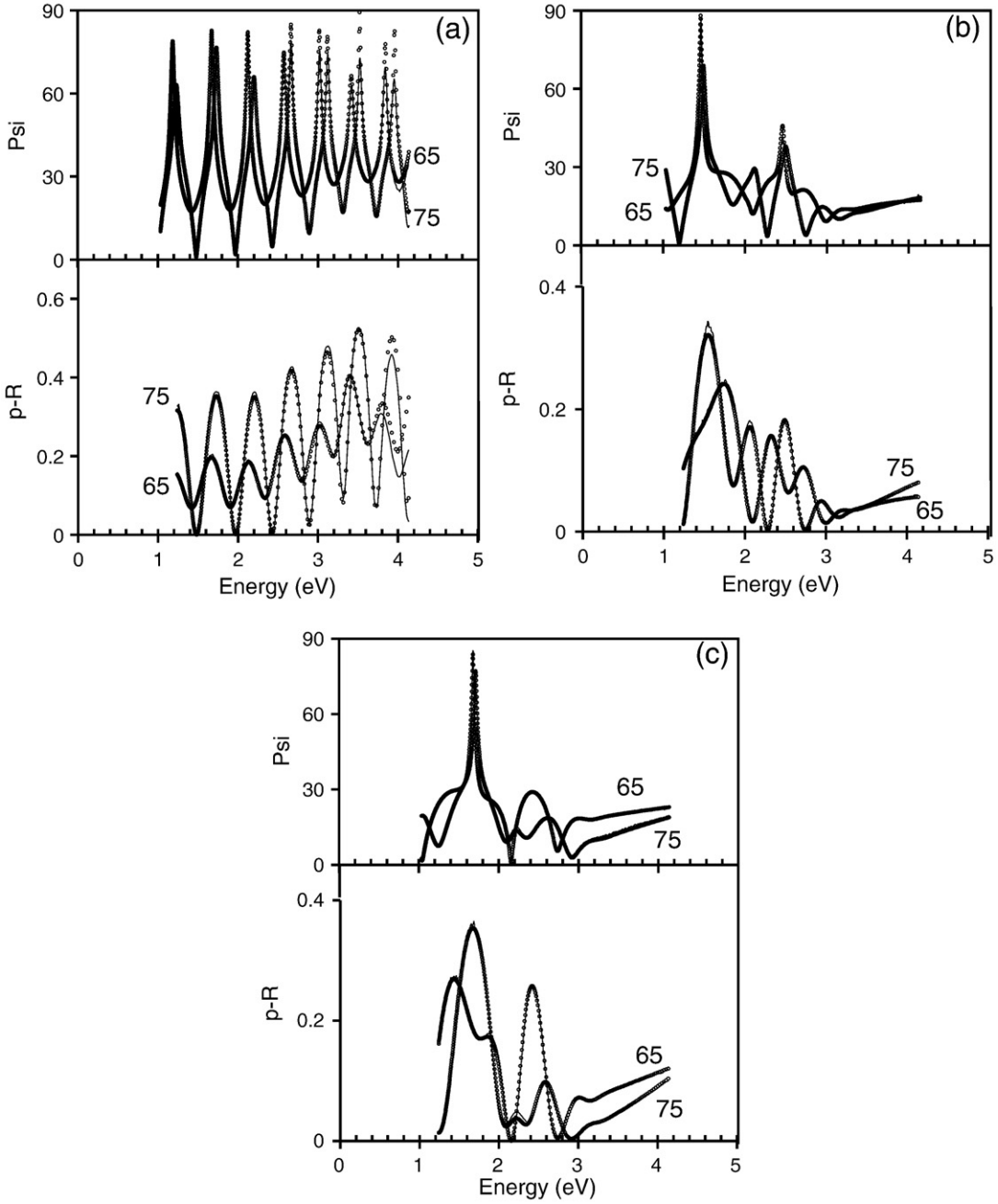

Fig. 1. Experimental (●) and modeled (—) results for the spectroscopic ellipsometry parameter (Psi) and p-polarized reflectance (p-R) for 65° and 75° angles of incidence for (a) $SiO_{0.96}N_{0.27}$:H (b) $SiO_{0.49}N_{0.19}$:H and (c) $SiO_{0.17}N_{0.07}$:H.

65° and 75°. VASE was also used to acquire p-polarized reflection (p-R) data from each sample at least one angle of incidence for ellipsometry data. A baseline data scan was performed before the main data scans.

Optical modeling and data analysis were done using the J.A. Woollam WVASE32 software package [7]. Ellipsometric data ψ and Δ for variable angles and wavelengths were fitted in the optical model. The p-polarized reflectance data was appended to the ellipsometry data and the model was refined to simultaneously fit the ellipsometry data and reflectance data.

GAXRD was performed using Bruker-D8 Discover with a Gobel mirror on the incident beam side and scintillation detector on the detector side. CuK_α radiation (E=8041.3 eV) was used for the GAXRD measurements. The experimental details for GAXRD have been published elsewhere [5,8]. GAXRD measurements in the 2-theta range 5–80° were performed at an angle of incidence of 0.5°. At this angle of incidence the depth penetration of X-rays for SiO_2 was estimated to be ~2.3 μm. The time per step for each measurement was 6 s.

XPS measurements were performed using a Physical Electronics 5800 Model instrument. A monochromatic Al k line of energy (1486.6 eV) was employed as the X-ray source. A pass energy of 23.5 eV was used for the measurements. The sample was progressively sputtered for 1 min using 2 kV Ar ions, to expose the underlying surface and scanned for the elemental composition. Under similar conditions the sputter rate of SiO_2 was found to be 1.6 nm/min. The integrated peak area intensities under O 1s, Si 2p, N1s and C1s peaks were used for estimating the atomic concentration as a function of thickness using each element atomic sensitivity factor. The background pressure during sputtering and measurement was lower than 2×10^{-6} Pa.

Scanning Electron Microscope (SEM) images were recorded using JSM-6500F, a field emission system with the In-Lens Thermal Field Emission Electron Gun. The operating voltage of SEM was 15 kV.

Fourier Transform Infrared (FTIR) transmission measurements in the spectral range 450–4000 cm^{-1} were carried out using a Thermo Nicolet MagnaIR 760 spectrophotometer equipped with a deuterated triglycine sulfate detector with KBr windows and an XT-KBr beam splitter. The spectral resolution for the measurements was 8 cm^{-1}. The sample compartment was purged with nitrogen.

The Photoluminescence (PL) data was taken using an Oriel InstaSpec IV CCD and the MS-257 Imaging Spectrograph, with the InstaSpec data acquisition software. The data were corrected for system response, neutral densities filters, and long pass filters. The laser used for excitation was a Kimmon IK Series He–Cd laser at 20 mW. An interference filter was used to pass only the laser line.

3. Results

Fig. 1a shows the experimental and fitted elllipsometry data Psi and p-R for a $SiO_{0.96}N_{0.27}$:H film deposited on a Si substrate with 500 nm interlayer. To model the complete structure, the optical constants of Si obtained by Jellison [9] were used for the substrate. The optical constants and a thickness of 500 nm SiO_2 inter were obtained separately by fitting the ellipsometric data with a Cauchy [10] layer. The thickness of this was allowed to vary for fitting purposes. The model for the $SiO_{0.96}N_{0.27}$:H (Fig. 1a) film, comprised of only a Cauchy layer. Finally a surface roughness was added to get the best fit. The introduction of an interface layer did not improve the fit, and hence was not used for this case.

The experimental and fitted elllipsometry and reflectance data for $SiO_{0.49}N_{0.19}$:H films is shown in the Fig. 1b. The various attempts to model this data assuming either a Cauchy or Effective Medium Approximation [10,11] layer did not yield reasonable fit.

The optical constants of the $SiO_{0.49}N_{0.19}$:H film were generated using a General Oscillator (Genosc) Layer [7]. The Genosc layer models the dielectric function of a film or substrate as a linear summation of real or complex terms (or "oscillators"), each of which is a function of wavelength (nm or μm), wave number (cm^{-1}), or photon energy (eV). Initially a Cauchy [10] layer model was used to estimate the thickness and refractive index of the $SiO_{0.49}N_{0.19}$:H film in the wavelength region of high transparency (for this case 600–1200 nm). Various Cauchy parameters and thicknesses were refined to fit the experimental data. A surface roughness and an interface layer composed of a-Si were introduced to get the best fit. The thickness of the $SiO_{0.49}N_{0.19}$:H film, and other films, obtained by fitting were used in the optical model of the

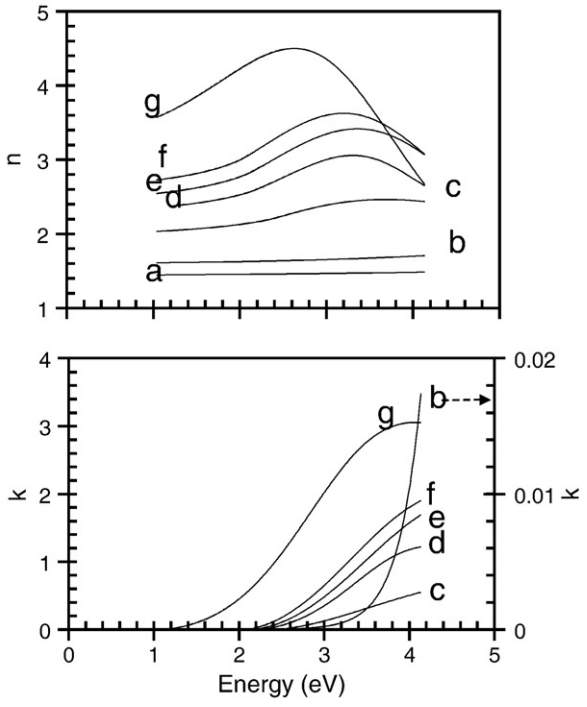

Fig. 2. The refractive index (n) and extinction coefficient (k) as a function of energy (eV) for (a) a-SiO_2 (b) $SiO_{0.96}N_{0.27}$:H (c) $SiO_{0.49}N_{0.19}$:H (d) $SiO_{0.29}N_{0.13}$:H (e) $SiO_{0.18}N_{0.09}$:H (f) $SiO_{0.17}N_{0.07}$:H and (g) a-Si layers.

Table 1
Best fit model for as-deposited and annealed SiO_xN_y/H ($0.17 \le x \le 0.96$; $0.07 \le y \le 0.27$) films

Composition	Annealing temperature °C	Surface roughness thickness (nm)	SRON layer thickness (nm)	Interface thickness (nm)	SiO_2 layer thickness (nm)	Si(100) substrate (mm)	n (2.07 eV)	E_g eV)	E_{04} (eV)	E_u (meV)
$SiO_{0.96}N_{0.27}$:H	30	1.5	529.7	–	509.4	1	1.6	–	–	246±5
	400	2.6	529.1	–	506	1	1.6	–	–	256±5
	600	2.0	515.6	–	502	1	1.7	–	4.0±0.1	309±5
	800	14.3	470.1	–	505.7	1	1.7	–	3.6±0.1	424±5
$SiO_{0.49}N_{0.19}$:H	30	7.1	293.3	0.6	515.4	1	2.1	2.4±0.1	2.7±0.1	110±10
	400	7.4	291.6	0.4	506.8	1	2.2	2.3±0.1	2.5±0.1	145±10
	600	9.2	250	0.7	508.4	1	2.6	2.1±0.1	2.2±0.1	126±10
	800	17.5	220.3	1.0	503.7	1	2.8	2.2±0.1	2.0±0.1	146±10
$SiO_{0.29}N_{0.13}$:H	30	4.9	195.0	1.2	518.3	1	2.6	2.3±0.1	2.4±0.05	96±10
	400	5.6	191.4	1.4	504.6	1	2.7	2.2±0.1	2.2±0.1	99±10
	600	6.2	161.9	3.1	504.9	1	3.2	2±0.1	2.0±0.1	83±10
	800	19.7	128.2	5.4	499.7	1	3.7	2.1±0.1	1.7±0.1	144±10
$SiO_{0.18}N_{0.09}$:H	30	3.1	148.6	1.9	519.4	1	2.8	2.2±0.1	2.3±0.1	42±10
	400	3.7	146.7	2	502.6	1	3.1	2±0.1	2.1±0.1	49±10
	600	4.2	125.7	3.8	504.7	1	3.6	1.9±0.1	1.9±0.1	51±10
	800	11.9	105.8	7.7	500.7	1	3.8	2±0.1	1.8±0.1	67±10
$SiO_{0.17}N_{0.07}$:H	30	2.3	127.6	1.2	516.2	1	3.0	2.1±0.1	2.3±0.1	56±10
	400	2.9	127.6	1.3	503.2	1	3.2	2±0.1	2.1±0.1	62±10
	600	3.4	110.8	1.2	505.1	1	3.8	1.9±0.1	1.8±0.1	88±10
	800	7.8	99.8	3.7	503.5	1	4.0	2±0.1	1.8±0.1	17±10

The as-deposited films are listed as 30 °C under the annealing temperature column. Values of various thickness and optical parameters are also listed. *Eg* (optical band gap); E_{04} (energy values where absorption coefficient (α) equals 10^4 cm^{-1}, E_u (Urbach Energy).

sample. In the next step, using the known "n" and "k" values determined in the high transparency region (longest wavelength), a wavelength-by-wavelength fit was performed over the entire spectral region. The point-by-point spectra of "n" and "k" obtained by this method over the entire wavelength region was then fitted with a general oscillator layer composed of a single *Tauc–Lorentz* (TL) oscillator [12,13]. Oscillator parameters like strength, center energy, broadening values, etc., were fitted to match the point-by-point spectra. The data was generated and compared with the experimental values. Finally, the difference between the experimental and modeled ellipsometry and reflectance data parameters were reduced by regression analysis.

A similar methodology was employed for the determination of thickness and optical constants of other as-deposited SRON films ($SiO_{0.29}N_{0.13}$:H, $SiO_{0.18}N_{0.09}$:H, and $SiO_{0.17}N_{0.07}$:H). The "n" and "k" values for all the SRON films obtained are shown in Fig. 2. The refractive index for a-Si and SiO_2 obtained using Palik's data [14] are also shown for comparison. As seen in the figure, with increased silicon content the refractive index of the film increased progressively. The thickness values for various films for each structure are shown in Table 1.

The GAXRD measurements were performed on annealed samples and did not reveal any peaks suggesting polycrystalline or nanocrystalline materials. Based on the XRD results it was concluded that the annealing conditions were insufficient to nucleate the formation of Si crystallites in the SRON film. Also, no discernable features were observed in the SEM images of the annealed films. The annealed SRON films were fitted using the approach for each as-deposited film. In the model, the surface roughness, film thickness, interface layer and SiO_2 layer were allowed to vary. Finally, the Cauchy or TL oscillator parameters were refined to get the best fit results. Fig. 3 shows the refractive index values for as-deposited and annealed SRON films. The thickness values for the annealed films are tabulated in Table 1.

We further investigated the dependence of the optical properties of these films on the composition and annealing conditions. The absorption coefficient "α"(cm^{-1}) is related to the extinction coefficient by the relation

$$\alpha = \frac{4\pi k}{\lambda} \tag{1}$$

Fig. 4 shows the dependence of the absorption coefficient on the photon energy for as-deposited and annealed films.

The absorption spectra of the films can be divided into two parts, a region of high absorption (also called the Tauc region) with $\alpha > 10^5$ cm^{-1} and a low absorption region (Urbach region) with typically $10 < \alpha < 10^5$ cm^{-1}. The spectral response in the Tauc region is attributed to the optical electron transition between the extended valence band and the conduction band [15]. The absorption in the Urbach region takes an exponential form and is due to optical transitions involving band tail states [15]. Tauc's extrapolation [16,17] method is typically used to estimate the optical band gap (E_g) from the spectrum in the Tauc's region. An inverse of slope of ln(α) vs energy is utilized to obtain Urbach energy (E_u) from the Urbach region.

Tauc's extrapolation method was used to estimate the optical band gap of all the as-deposited and annealed films other than $SiO_{0.96}N_{0.27}$:H. The as-deposited and annealed $SiO_{0.96}N_{0.27}$:H films did not exhibit a large enough absorbance, in the optical region of our studies, for this extrapolation. It is likely that these

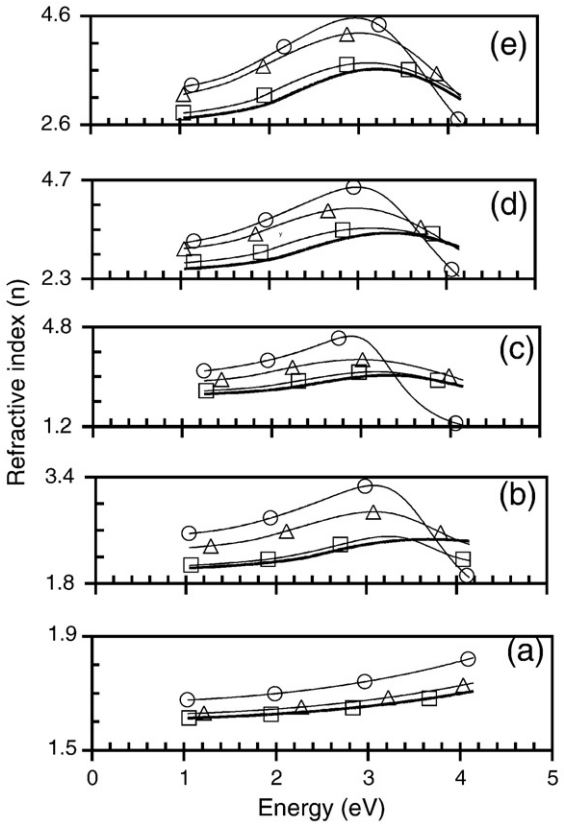

Fig. 3. The refractive index (n) as a function of energy of as-deposited and annealed SRON layers. (a) $SiO_{0.96}N_{0.27}$:H (b) $SiO_{0.49}N_{0.19}$:H (c) $SiO_{0.29}N_{0.13}$:H (d) $SiO_{0.18}N_{0.09}$:H (e) $SiO_{0.17}N_{0.07}$:H. Data for annealed films is represented as (—□—) 400 °C (—Δ—) 600 °C (—O—) 800 °C for 4 h under inert conditions. As-deposited film is represented by heavy solid line only (− −).

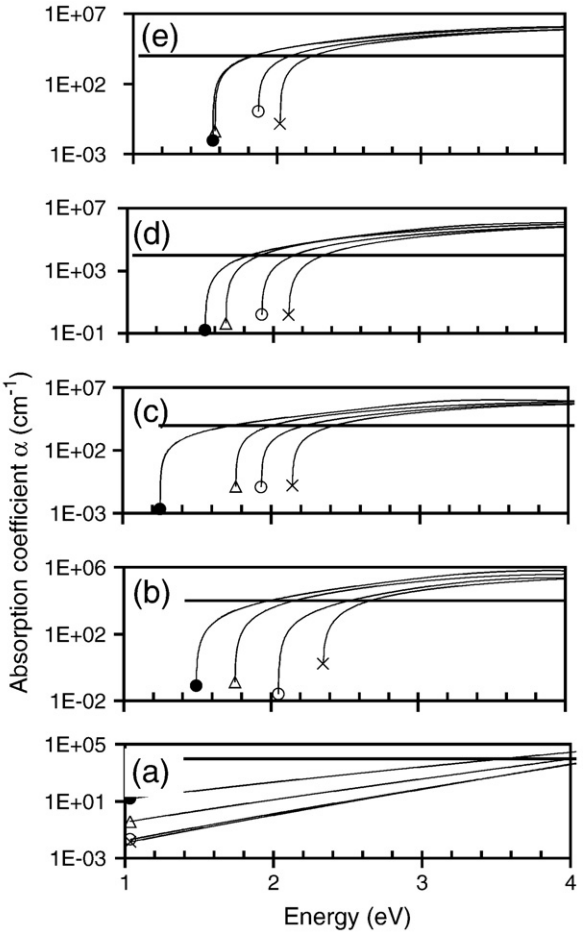

Fig. 4. The absorption coefficient as a function of energy plotted on a log scale for (a) $SiO_{0.96}N_{0.27}$:H (b) $SiO_{0.49}N_{0.19}$:H (c) $SiO_{0.29}N_{0.13}$:H (d) $SiO_{0.18}N_{0.09}$:H (e) $SiO_{0.17}N_{0.07}$:H. Data for annealed films is represented as (O—) 400 °C (Δ—) 600 °C (●—) 800 °C for 4 h under inert conditions. The as-deposited film is represented by (X—). The solid horizontal line represents values where $\alpha = 10^4$ cm^{-1}.

films had a band gap much higher than 4.1 eV (the maximum spectral range used). The values of E_{04} (energy values corresponding to an absorption of 10^4 cm^{-1}) were also determined from the data. Finally the values of E_u were determined and are listed in Table 1.

Fig. 5 shows the XPS depth profile analysis of $SiO_{0.17}N_{0.07}$:H films sputtered for 25 min. The results clearly indicate the uniformity of the film composition across the film thickness.

As seen in our previous study [4], SRON films had hydrogen bonded to silicon in these films. High temperature annealing under inert conditions is likely to cause diffusion of hydrogen out of the film. Fig. 6 a–c shows the FTIR spectra of Si–H stretching peak in the range 2000–2200 cm^{-1}. As seen in the figure, while the Si–H stretch could be seen in the films annealed at 400 °C, the FTIR spectra of the films annealed at 600 °C were devoid of the Si–H stretching mode. This signifies complete diffusion of hydrogen out of the film as a result of annealing at 600 °C.

The room temperature PL spectra for as-deposited films has been discussed in the past [4]. The data for RT PL has been reproduced here for the sake of comparison. The as-deposited films had different film thicknesses. In order to investigate the effect of volume fraction on the intensity of PL spectrum, the PL spectra for each film was divided by the respective film thickness in nanometers. Fig. 7 shows the spectra of SRON films normalized for the film thicknesses. As seen in the figure, the SRON films with $x < 0.49$ had relatively stronger PL as compared to films with $x \geq 0.49$.

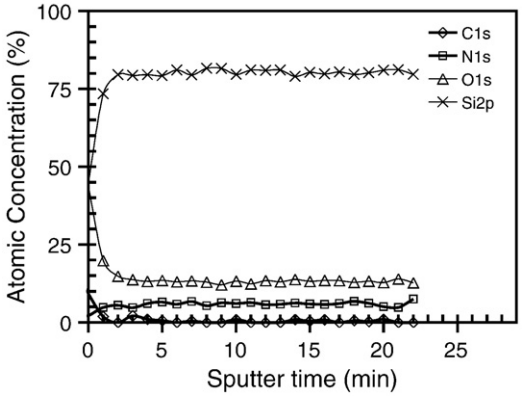

Fig. 5. XPS depth profile analysis of $SiO_{0.17}N_{0.07}$:H layer.

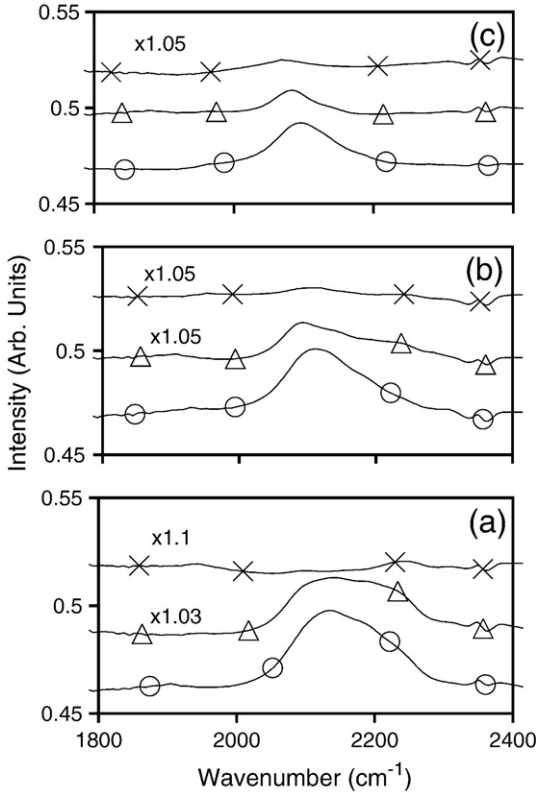

Fig. 6. FTIR absorbance spectra of SRON films showing Si–H stretching peak for as-deposited and annealed layers. (a) $SiO_{0.96}N_{0.27}$:H (b) $SiO_{0.29}N_{0.13}$:H (c) $SiO_{0.17}N_{0.07}$:H. (O) As-deposited, and annealed at (Δ) 400 °C and (X) 600 °C.

Fig. 8 shows the comparison of the PL spectra of as-deposited and annealed SRON films. These results are detailed below.

In the case of the as-deposited $SiO_{0.96}N_{0.27}$:H film, the PL signal was comprised of broad PL peaks at 1.7 and 2.0 eV with the high energy (HE) peak being more intense than the low energy (LE) peak. As the film was heated to 400 °C, PL peaks at 1.8 and 2.2 eV were seen. As the film was further heated to 600 °C, while the PL peak energies remained nearly constant, the intensity of the PL signal increased. With the further increase of the annealing temperature to 800 °C, PL peak energy still did not change. However, annealing at 800 °C not only resulted in further increase of the PL intensity, but it also resulted in additional luminescence peaks at energies greater than 2.2 eV. —

The as-deposited $SiO_{0.49}N_{0.19}$:H film had PL peaks centered on 1.6 and 2.0 eV with the HE peak being more intense than the LE. As this film was annealed to 400 °C, the intensity of the HE component was reduced while the LE component remained about the same. No change in the PL peaks energy was seen. The PL signal was substantially reduced for the $SiO_{0.49}N_{0.19}$:H film heated to 600 °C and the peaks were shifted towards lower energies (1.5 and 1.8 eV). However, as this film was further annealed to 800 °C, the PL peaks centered on 1.9 eV & 2.1 with a shoulder peak at 1.6 eV were observed.

Also, in the case of the as-deposited $SiO_{0.29}N_{0.13}$:H film, the LE (1.4 eV) PL peak was less intense than the HE component (1.7 eV). As this film was annealed at 400 °C, the PL signal was reduced by a factor of 10 and the peaks were also red shifted (Fig. 8c). However, in the case of the film annealed at 600 °C, no discernable PL signal was observed. As the film was further heated to 800 °C, PL peaks at energies greater than 2.0 eV were seen.

In the case of the as-deposited $SiO_{0.18}N_{0.09}$:H film, a broad PL peak centered on 1.4 eV was seen. As the sample was heated to 400 °C not only the red shift of the luminescence peaks was evident, also the intensity of PL signal was reduced by an order

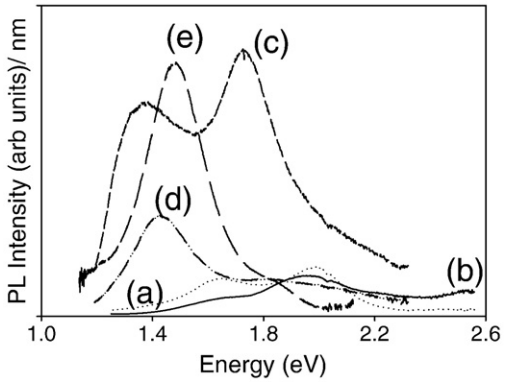

Fig. 7. RT PL spectra of as-deposited layers normalized for individual layer thickness. (a) $SiO_{0.96}N_{0.27}$:H (b) $SiO_{0.49}N_{0.19}$:H (c) $SiO_{0.29}N_{0.13}$:H (d) $SiO_{0.18}N_{0.09}$:H (e) $SiO_{0.17}N_{0.07}$:H.

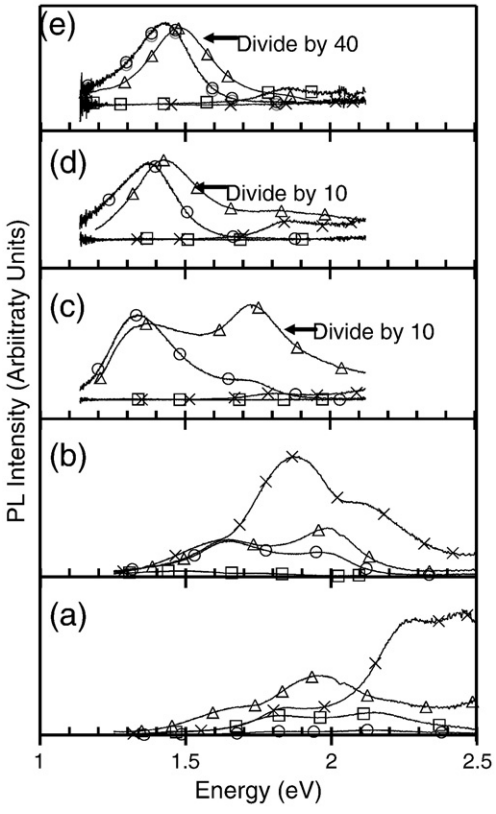

Fig. 8. Room temperature PL spectra of (a) $SiO_{0.96}N_{0.27}$:H (b) $SiO_{0.49}N_{0.19}$:H (c) $SiO_{0.29}N_{0.13}$:H (d) $SiO_{0.18}N_{0.09}$:H (e) $SiO_{0.17}N_{0.07}$:H layers. (Δ) as-deposited; annealed at (O) 400 °C, (□) 600 °C and (X) 800 °C.

of magnitude. No RT luminescence was observed for sample heated to 600 °C. Finally, high energy PL was seen for the film annealed at 800 °C.

A similar PL response was also observed for as-deposited and annealed $SiO_{0.17}N_{0.07}$:H, films. However, in this case the PL signal from the film annealed at 400 °C was lower than the as-deposited film by a factor of 40.

4. Discussion

The as-deposited SRON films prepared in these studies were amorphous in nature. The optical constants "n" and "k" of the $SiO_{0.96}N_{0.27}$:H film varied as a function of wavelength, λ. In comparison to standard SiO_2, the refractive index of $SiO_{0.96}N_{0.27}$:H was significantly higher and also exhibited non-zero absorbance. The non-zero absorbance was likely a consequence of a high concentration of Si–Si bonds since Si–N, Si–O, Si–H, or N–H bonds are unlikely to contribute to the extinction coefficient of the film [18].

With increased silicon content in the SRON film ($SiO_{0.49}N_{0.19}$:H), the density of Si–Si bonds in the film increased. This assumption is supported by our earlier studies where it was observed that not only were elemental Si features present in the XPS of the SiO_xN_y films with $x<0.96$, but the $SiO_{0.96}N_{0.27}$:H and $SiO_{0.49}N_{0.19}$:H samples also had similar values of high energy and low energy Photoluminescence (PL) peak maxima [4]. This is possible due to the increased volume fraction of embedded amorphous silicon clusters in the $SiO_{0.49}N_{0.19}$:H samples with sizes similar to those of clusters in the $SiO_{0.96}N_{0.27}$:H sample. As result of the increased Si–Si bonds, the $SiO_{0.49}N_{0.19}$:H film had a significantly higher absorption, as compared to $SiO_{0.96}N_{0.27}$:H film. With the progressive increase of silicon content in $SiO_{0.29}N_{0.13}$:H, $SiO_{0.18}N_{0.09}$:H, and $SiO_{0.17}N_{0.07}$:H films, the diameter and the volume fraction of these silicon clusters increased as well. This assumptions is consistent with our earlier reported results [4], where not only did we observe that the relative area of the elemental silicon peak increased with increasing silicon composition for the sample with $x<0.96$, but we also observed a red shift of the PL peak maxima. Therefore, this increase in the size and volume fraction of the silicon clusters was responsible for the increased absorbance in these films. Another noticeable component of the SRON films, aside from the $SiO_{0.96}N_{0.27}$:H film, was the presence of a thin, high-refractive interface film of a-Si between the SRON and SiO_2 film. This film, in principle, signified the presence of a high-refractive index film with optical constants higher than silicon nitride and SiO_2 film. The interface film was likely a result of excess silicon at the interface formed during the deposition process.

The absence, of crystalline features in the GAXRD pattern of annealed SRON films indicated that the annealing conditions in the present study were insufficient to nucleate the silicon nanocrystals. We observed that annealing caused the compression of the SRON film accompanied by increased values of the refractive indices and extinction coefficients. A comparison of FTIR spectra of as-deposited and annealed films indicated an absence of Si–H bonds in our annealed films (Fig. 6). This was a result of hydrogen diffusing out of the films during the annealing process. Hydrogen diffusion has led to an apparent reduction in thickness and densification of the films. This caused an increase in the values of the optical constants (n and k). No changes were seen in the thickness of the SiO_2 interlayer.

The Urbach energy parameter, E_u, represents quantitative characteristics of the static disorder in an amorphous structure and reflects the band tails extent of the density of electron states. The changes in E_u represent irreversible microstructural changes in the amorphous material. This increase can indicate larger disorder in the structure as well as the formation of new defects. In the example of as-deposited films with increased silicon concentration, the values of E_u decreased progressively, signifying increased order in these films. In films other than $SiO_{0.17}N_{0.07}$: H the value of E_u increased with increased annealing temperatures. This is possibly due to hydrogen evolution, film compaction, and changes in the microstructure of the film that has added to disorder in the SRON film. However, in case of $SiO_{0.17}N_{0.07}$:H the value of E_u dropped sharply for the film annealed at 800 °C. It is likely this film underwent some increased ordering at this temperature. However, the GAXRD patterns did not show the presence of any crystalline features. We believe that the films underwent some ordering, but not enough to be observed in the GAXRD patterns.

The E_g and E_{04} were found to decrease with increased silicon content and annealing temperatures. It must be noted that for as-deposited films, while a decrease in band gap *in excess* of 1.4 eV was observed as x decreased from 0.96 to 0.49 ($\Delta x=0.47$), only a decrease of 0.3 eV was observed as x decreased from 0.49 to 0.17 ($\Delta x=0.32$). Similar trends were seen for the annealed samples. E_{04} values also exhibited similar trends as a function of composition and annealing temperature. A correlation was seen between the changes in the refractive index, E_{04} and E_u as a function of composition and annealing conditions.

Our films are a complicated hydrogenated mixture of Si, O and N [4]. In the past, the RT PL spectrum of SRON films was attributed to the presence of embedded amorphous silicon clusters [4,19]. The presence of more than a single luminescence peak was attributed to different average sizes of the embedded clusters [4]. The amorphous silicon clusters are embedded in the Si–O–N dielectric and silicon defects passivated by hydrogen. The intensity of the PL signal of the as-deposited film is governed by the volume fraction of the silicon content (silicon clusters) and the fraction of silicon clusters contributing to the PL signal (Fig. 7). Also, the PL peak energy is dependent on the size of the embedded clusters. As the films were heated, the bonded hydrogen diffused out of the film, leading to the formation of defects. These defects act as centers for non-radiative recombination, thus reducing or quenching the PL signal. The relative extent of reduction in the PL signal is largely governed by the concentration of hydrogen bonded to silicon. For example as compared to $SiO_{0.49}N_{0.19}$:H, the $SiO_{0.29}N_{0.13}$:H film is likely to have a larger concentration of bonded hydrogen. Thus when the $SiO_{0.29}N_{0.13}$:H film is annealed, comparatively more hydrogen diffused out of the

film. Thus in such a scenario, more defects are likely to be formed in $SiO_{0.29}N_{0.13}$:H as compared to $SiO_{0.49}N_{0.19}$:H. This led to a stronger reduction of the PL signal in the former. The increased silicon content is apt to increase the likelihood of coalescence of the embedded silicon clusters causing the PL to red shift. At the same time, films with higher oxygen content or lower silicon content have concomitant higher nitrogen content. As seen in previous studies, presence of nitrogen in these films plays an important role in the silicon nucleation and coalescence kinetics [5]. Presence, of the strong Si–N bond, prevents the coalescence of small-embedded clusters into clusters of larger diameter. Besides, the presence of amorphous silicon clusters, defects in these SRON films can also contribute to the RT luminescence. In the literature, the PL peak around 4.4 eV has been attributed to an oxygen-deficient defect, while the peaks around 3.5 and 2.4 eV are related to oxygen-excess defects [20]. The PL peak around 1.9 eV in glassy SiO_2 has also been related to an oxygen-excess defect and is induced in all glassy SiO_2 exposed to various ionizing irradiations, ion implantations or mechanical stresses. In the past we attributed the presence of oxygen related defects in the Si–O system to be the origin of the 2.5 and 1.9 eV PL peaks in annealed $SiO_{0.17}N_{0.07}$:H film [5]. In the light of aforesaid data, the effects of annealing on the RT luminescence of SRON films can be described as follows.

In the case of the $SiO_{0.96}N_{0.27}$:H film, as the sample was heated, the hydrogen diffused out of the film leading to the formation of defects in the film. The PL peaks for annealed films were blue shifted as compared to the as-deposited film. Since, the PL peak energies were independent of the annealing temperatures, as well as the intensity of the PL peaks increased with increasing annealing temperatures, we concluded, that the PL peaks at 1.8 and 2.2 eV were a result of possible oxygen related defect formation in the annealed films.

The $SiO_{0.49}N_{0.19}$:H film had considerably higher content of silicon (thus higher bonded hydrogen) and lower nitrogen content (thus lower concentration of Si–N bonds) as compared to $SiO_{0.96}N_{0.27}$:H. As the $SiO_{0.49}N_{0.19}$:H film was heated to 400 °C, the hydrogen diffused out leading to the formation of large defects in the film and thus reducing the PL signal. Lack of any change in the PL peak energies signified the constancy of the silicon cluster size. Presence to Si–N bonds probably prevented the coalescence of silicon clusters at this stage. However, further heating of the film to higher temperature (600 °C) led to the complete diffusion of hydrogen out of the film. At this stage, the annealing conditions were conducive enough to cause the coalescence of the embedded silicon clusters. This led to the observed reduction and red shift of the PL spectrum. With still higher annealing temperatures (800 °C), the PL signal was likely a result of defects in the silicon sub oxide phase in the film.

As compared to the previous two samples, the $SiO_{0.29}N_{0.13}$:H film had even higher silicon content and lower nitrogen content. As this film was heated to 400 °C, large quantities of hydrogen diffused out of the film. This led to the formation of a greater number of unpassivated defects as compared to the previous two films, under similar annealing conditions. The presence of a high silicon content and low nitrogen content at this stage was conducive enough to cause coalescence of silicon clusters at a temperature as low as 400 °C. This led to significantly reduced and red shifted PL spectra at 400 °C only. Further increasing the annealing temperature (600 °C) resulted in no significant luminescence signal being observed. This was likely a result of complete hydrogen evolution leading to the formation of large number of unpassivated defects. However, for the film heated to 800 °C the luminescence signal was likely a result of oxygen related defects in the silicon sub oxide phase in the SRON film. The effect of annealing on the RT PL signal for the $SiO_{0.18}N_{0.09}$:H and $SiO_{0.17}N_{0.07}$:H, films were similar to those for the $SiO_{0.29}N_{0.13}$:H film. As compared to the as-deposited films (Fig. 6 b–d), for the films annealed at 400 °C, the relative red shift of the PL peak maxima increased with increased silicon content and reduced nitrogen content.

5. Conclusion

As-deposited and annealed amorphous SiO_xN_y/H ($0.17 \leq x \leq 0.96$; $0.07 \leq y \leq 0.27$) films were characterized by spectroscopic ellipsometry in the UV–VIS–NIR range. With increased silicon content, the refractive index of as-deposited films could be successfully varied between SiO_2 and a-Si. It is likely this increased refractive index was a result of the increased volume and size of silicon clusters incorporated in the film. The annealing conditions were insufficient to nucleate the formation of Si crystallites in the SRON films. High temperature annealing led to the reduction of thicknesses, and an increase in the values of the optical constants (n and k) of the films. The optical band gap and E_{04} showed a decrease in value with increasing silicon content. A correlation was seen between the changes in refractive index, E_{04} and E_u as a function of composition and annealing conditions. However, a noticeable exception was $SiO_{0.17}N_{0.07}$:H. It is postulated that this film underwent increased ordering when annealed at 800 °C. The effect of annealing conditions on the room temperature PL response of SRON films has been investigated. The RT luminescence in annealed $SiO_{0.96}N_{0.27}$:H films was attributed to the formation in oxygen related defects in these films. In other films, the amount the bonded hydrogen as well as silicon and nitrogen content played an extremely important role in determining the influence of annealing conditions on the room temperature PL spectra. Evolution of bonded hydrogen from the film, as a consequence of annealing, led to the formation of unpassivated defects in the film that led to a diminished/quenched PL signal. The more bonded hydrogen in the as-deposited film, greater the relative reduction/quenching of the PL signal. The shift in the PL peak maxima, as a result of annealing conditions, was largely governed by the silicon and nitrogen content in the as-deposited film. It is postulated that the presence of strong Si–N bonds in the film played an important role in PL peak maxima shift.

Acknowledgements

Authors acknowledge the financial support provided by the NSF instrument Grant Nos. NSF-CHE-9808024 and NSF-DMR-0076180.

References

[1] M.L. Green, E.P. Gusev, R. Degraeve, E.L. Garfunkel, J. Appl. Phys. 90 (2001) 2057.
[2] K. Worhoff, L.T.H. Hilderink, A. Driessen, P.V. Lambeck, J. Electrochem. Soc. 149 (2002) F85.
[3] E. Desbiens, R. Dolbec, M.A. El Khakani, J. Vac. Sci. Technol., A, Vac. Surf. Films 20 (2002) 1157.
[4] S. Kohli, J.A. Theil, P.C. Dippo, R.K. Ahrenkiel, C.D. Rithner, P.K. Dorhout, Thin Solid Films 473 (2005) 89.
[5] S. Kohli, J.A. Theil, P.C. Dippo, K.M. Jones, M.M. Ai-Jassim, R.K. Ahrenkiel, C.D. Rithner, P.K. Dorhout, Nanotechnology 15 (2004) 1831.
[6] J.A. Theil, G.A. Kooi, R.P. Varghese, Europe Patent No. 1164206, 30 Mar. 2001.
[7] Guide to Using WVASE32™, J. A. Woollam Co. Inc, Lincoln, NE, 1997.
[8] S. Kohli, J.A. Theil, R.D. Snyder, C.D. Rithner, P.K. Dorhout, J. Vac. Sci. Technol., B 21 (2003) 719.
[9] G.E. Jellison, Opt. Mater. 1 (1992) 41.
[10] H.G. Tompkins, A User's Guide to Ellipsometry, Academic Press, Boston, 1991.
[11] D.E. Aspnes, Thin Solid Films 89 (1982) 249.
[12] G.E. Jellison, F.A. Modine, [Erratum], Appl. Phys. Lett. 69 (1996) 2137.
[13] G.E. Jellison, F.A. Modine, Appl. Phys. Lett. 69 (1996) 371.
[14] E.D. Palik (Ed.), Handbook of optical constants of solids, Academic Press, San Diego, 1997.
[15] K. Tanaka, E. Maruyama, T. Shimada, H. Okamoto, Amorphous Silicon, Translated by T. Sato, John Wiley & Sons Ltd, Chichester, 1999, p. 118.
[16] J. Tauc, R. Grigorov, A. Vancu, Phys. Status Solidi 15 (1966) 627.
[17] N.F. Mott, E.A. Davis, Electronic processes in noncrystalline materials, Clarendon Press, Oxford, 1979, p. 273.
[18] H.G. Tompkins, R.B. Gregory, P.W. Deal, S.M. Smith, J. Vac. Sci. Technol., A, Vac. Surf. Films 17 (1999) 391.
[19] M. Ribeiro, I. Pereyra, M.I. Alayo, Thin Solid Films 426 (2003) 200.
[20] T. Kanashima, M. Okuyama, Y. Hamakawa, Jpn. J. Appl. Phys. 1 (35) (1996) 1445.